measurement of slope movement which measures the expansion and contraction between two measuring points with the help of stretched invar wire. Laser beam-optical sensor measures the displacements in vertical and horizontal directions with the help of laser beam source and matrix positioned laser receiving optical sensor (refer to Ito et al., 2006). Excavation was started from the toe of the embankment using a back hoe. Excavation was done by inserting the blade on the slope surface vertically downward up to the base and then pulling the blade away from the slope. The width of each cut of excavation was 0.5m and the time interval between two excavation steps was around 5 minutes. Excavation was done until the failure of whole slope took place. For both the embankments, excavation was done up to 6th cut where failure was observed.

2. Centrifuge models

Excavation of field embankments was simulated in the centrifuge. For this, Mark-II centrifuge (Horii et al. 2006) was used. Before preparing the slope models, Narita sand was thoroughly mixed with water content so that water content became almost same as that of filed embankment. Several trial compactions were done to make the wet density of centrifuge model slope equal to those of the field embankments. At the beginning, 5cm thick Kanto loam layer was prepared to represent the natural base as that in field by compacting it under 150 kPa. After this, 20 cm thick model slope ground was prepared in layers. To have uniform density throughout slope, model ground was prepared in 10 layers and 5 minute compaction time was allowed for each layer. In between each layer, NSF clay powder was spread so that inner movement of slope could be observed during excavation and after the failure. Static compaction was done using a bellofragm cylinder. As in the field, here also, two types of centrifuge slope models were prepared. Compaction pressure, wet density and water content for NSL and NSH type centrifuge slope models are shown in Table 1.

Table 1 Centrifuge model test condition.

Embankment type	Compressive stress	wet density	water content
	(kPa)	ρ_t(g/cm^3)	w (%)
NSL	193	1.4	26.1
NSH	265	1.7	25.6

Once the compaction was over, then two sides (wall) of the model box were removed and the model ground was cut to desire slope angle. Dimensions of the model ground are shown in Fig. 4. Here, all the dimensions are scaled to 1/25 to field embankment. Then two sides of the model ground were replaced by glass walls which were provided the marked rubber membranes and thin film of grease which helps to reduce the friction between the glass walls and the model ground. Whole the model box along with model slope was then lowered down on to the centrifuge platform. Linear vertical differential transducers (LVDTs) were set up on the slope top to measure the vertical deformation during the excavation (Photo 2). In case of NSL, they were set up at 1, 4.5, 7.5 and 11cm distances from the slope crest where as for NSH, they were set at 1, 4.5, 7.5 and 10.5cm from the slope crest. LVDTs are generally set up after placing the in-flight excavator above the centrifuge model box.

In-flight excavator (Toyosawa et al., 2000) which can move its blade freely in the vertical (up and down) and horizontal (forward and backward) directions during the running of the centrifuge was used. Since the width of the centrifuge model ground was 20cm, excavating blade of similar size (little less than 20cm) was used. Centrifuge acceleration was then increased in steps from 5, 10, 15, 20, to 25g. Once the deformation became constant at 25g, then excavation was started. Here, to match the field

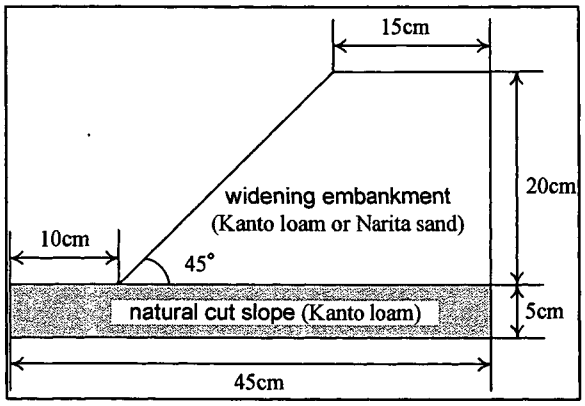

Fig. 4. Dimension of centrifuge model.

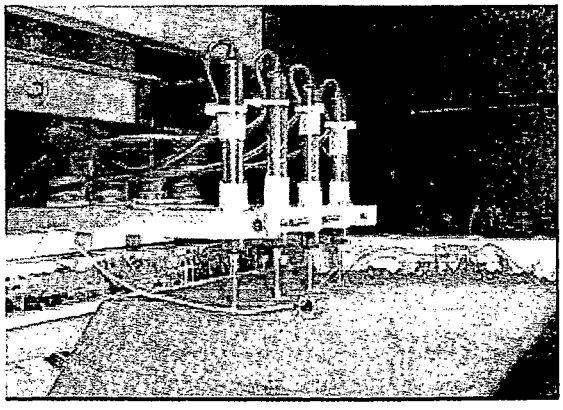

Photo 2. LVDT set up on the top of the model.

embankment, excavation width was maintained at 2cm (in proto type, 0.5m) and excavation was started from the toe of the slope down up to the surface of the hard base layer (resembles of natural slope of field). Vertically downward and then backward pulling of the blade was done in each step. About 2 minute waiting time was allowed after each step of excavation so that the deformation could be observed. Excavation was done until the failure occurred. In case of NSL, failure was seen after 6th cut where as no failure was observed even after 8th cut for NSH. Hence trench excavation of 0.5m x 0.5 m was done and acceleration was increased up to 26g. Failure was seen after this.

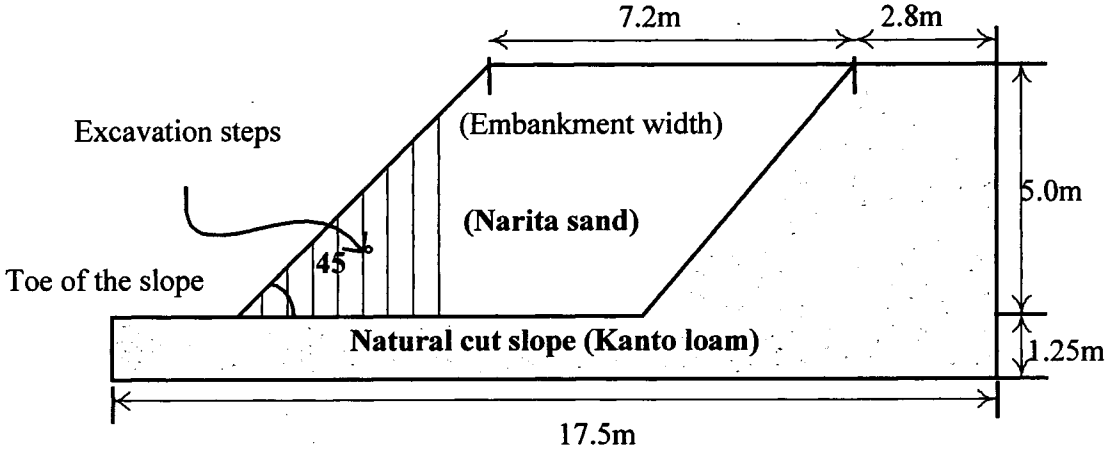

Fig. 5. Outline of the model slope considered for numerical analysis.

3. Numerical analyses

To understand the failure mechanism of model ground during failure, finite element analyses of model tests were carried out. Here, PLAXIS 2D software is used and Elastic-perfectly plastic Mohr Coulomb model was assumed. Fig. 5 shows the outline of the numerical model ground. Here, the dimensions of the model analyzed were same as those of the field embankments. During the analysis, movements along the horizontal direction for two sides of the model were considered to be fixed. Similarly, movements along horizontal and vertical directions at the base were considered to be fixed. Step wise excavation was done during the analysis. In Table 2, the parameters required to run the analysis are shown. For the natural cut slope, high stiffness value was considered. For normal slope, parameters were obtained either from the laboratory tests or from the field tests. Unit weight was obtained from core cutter and sand pouring method in the field. Where as cohesion and angle of shearing were obtained from direct shear test (drained values were used). Similarly, the Young's modulus was estimated from the N-values using the chart given by Schultze and Menzenbach (refer to Geotechnical engineering memo). For this, average N-value was estimated using the equation ($N = 0.002W_{sw} + 0.067N_{sw}$) given by Okada et al. (1992). W_{sw} and N_{sw} in the equation represent the weight of the loading and half-rotation number per 1m penetration, respectively. For N-values, Swedish weight sounding tests and portable dynamic cone penetration tests were conducted at the field.

Table 2. Soil parameters for numerical analysis.

	Natural cut slope (Kanto loam layer)	NSL	NSH
General properties			
γ_t (kN/m^3)	30.71	15.40	16.40
Permeability			
k_x (m/day)	0.02	8.64	8.64
k_y (m/day)	0.02	8.64	8.64
Stiffness			
E (kN/m^2)	8000	4512	4850
ν	0.35	0.35	0.35
Strength			
c (kN/m^2)	70.00	3.54	7.68
ϕ (°)	5.00	35.88	36.34

4. Results and discussions

4.1 Embankment excavation results

Photos 3(a) and 3(b) show the embankments after failure for NSL and NSH, respectively. In

case of NSL, partial failure was observed after 4th and 5th cuts and final large failure was observed after 6th cut at around 40.5 minutes of elapsed time. Similarly, for NSH, partial failure was observed after 5th cut and final large failure was observed after 6th cut at around 51 minutes of elapsed time. In both cases, tensile crack was appeared on the slope top which increased with the increase in the excavation step. Although final failure was occurred after 6th cut in both the cases, the time elapse of the highly compacted embankment (NSH) was little longer than that for the loosely compacted embankment (NSL).

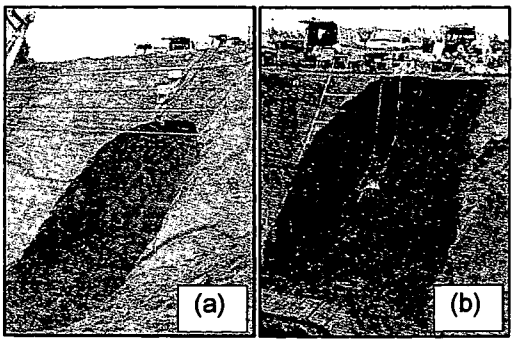

Photo 3. Embankments after failure (a) NSL and (b) NSH.

In Fig. 6(a) and 6(b), measurements of invar wire and laser beam-optical sensors with the increment in the step of excavation are shown. In both the cases, deformations measured with these instruments show almost similar trend and values. Measurements for first few steps were very small. But the measurement increased gradually after 4th and 5th steps (partial failure) and sharply and steeply after 6th step (final failure). Measurement made from both the instruments showed almost similar pattern. From the invar wire measurement results, rapid increment in the movement after 5th cut was seen and failed after 6th cut. Whereas for the NSH, gradual increment in the movement was seen from the 3rd step which keep on increasing even after 5th cut, showing the rapid increment after 6th cut. Difference in the time elapse for final failure was observed due to the difference in the degree of compaction.

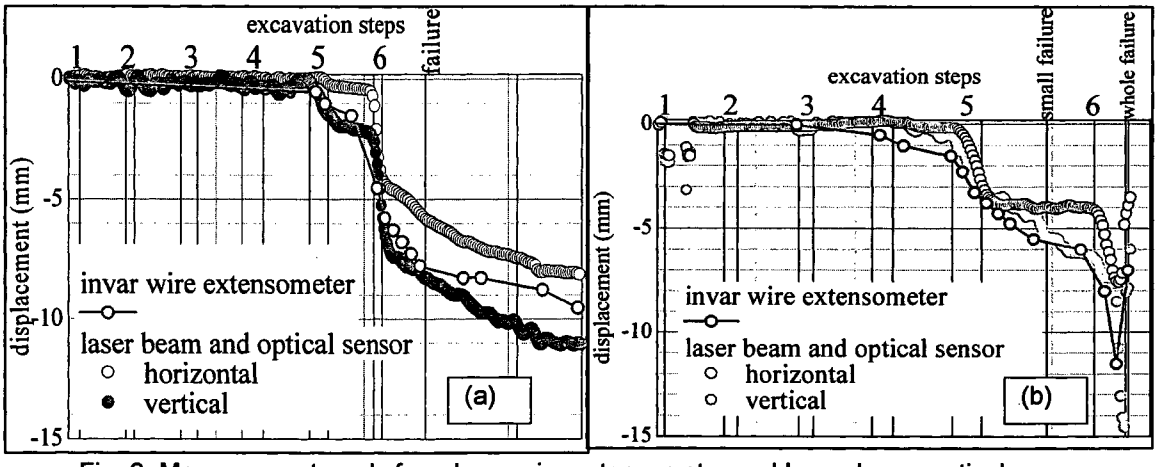

Fig. 6. Measurement made from Invar wire extensometer and Laser beam-optical sensor (a) NSL and (b) NSH.

4.2 Centrifuge excavation results

NSL centrifuge model was failed after 6th cut. In contrary to NSL, NSH model no failure was observed even after 6th cut. Hence failure was extended up to 8th cut. Although crack was seen on the slope top, still no failure occurred. Then trench excavation (0.5m x 0.5m) was done. As no increase in deformation was seen, then the centrifuge acceleration was increased up to 26g and slope failure was occurred. Fig. 7(a) and 7(b) show the deformation measured by LVDTs for NSL and NSH model slopes; respectively. Here, initialization of data was done when the deformation became constant at 25g. All the LVDTs showed the increment in deformation value with the increase in excavation step. LVDT placed closest to the slope showing the maximum values. Maximum value of deformation for both the slope model was around 15cm. In addition, they show similar pattern of movement. Deformation values shown in the figures are in proto type scale. Tension cracks were appeared in these tests as in the field tests.

4.3 Numerical analysis results

In Figs. 8(a) and 8(b), movement of "plastic points" from the toe of the slope towards the slope top and the development of "tension cut off points" on the slope top with the advancement of

excavation steps are shown. Plastic points represent the zone of where soils are in plastic condition. Similarly, tension cut off points show the zone where soils tend to collapse by tension.

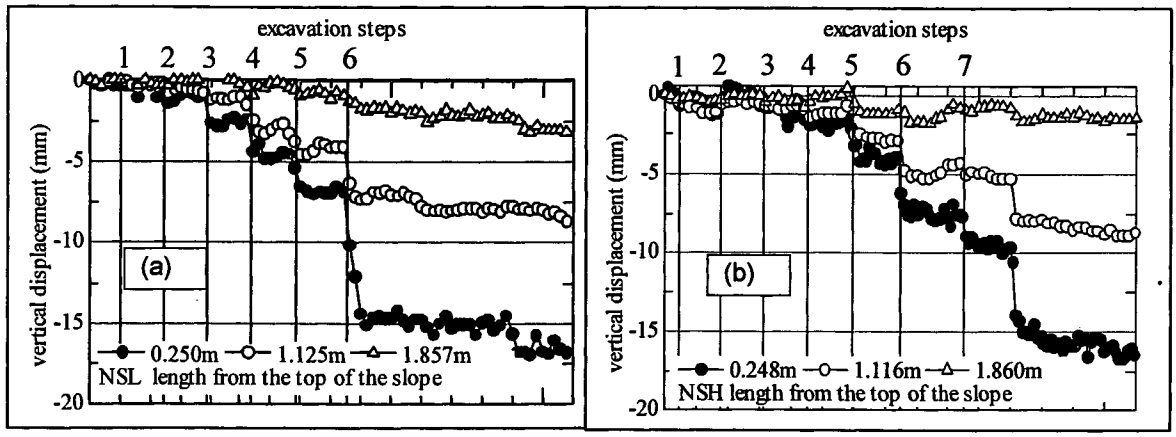

Fig. 7. Deformation measured by LVDT on the slope top of centrifuge models (a) NSL and (b) NSH.

In the case of NSL (Fig. 8(a)), plastic points were appeared after 1st step of excavation and these points increased with the increase in excavation steps. The zone of plastic points increased towards the slope top with the advancement excavation. Tension cut off points were appeared at the start. But the zone of these tension points on decreased with the advancement of excavation. In contrary, plastic points appeared at the slope also. Later on, increasing plastic points at slope toe and appearing plastic points on slope top meet with each other and the complete failure of the slope occurred. In case of NSH (Fig. 8(b)), both plastic points and tension cut off points appeared from the beginning. Here, with the increase in excavation steps, zone of plastic points increases. But no plastic points appeared on the slope top as in NSL. Instead the zone of tension cut off points increased. These shows why there is difference in the failure pattern of highly compacted (NSH) and loosely compacted slopes (NSH). In the field, in case of NSL, failure within the slope was only seen. No failure up to the slope top was observed despite tensile cut was seen on the slope top. In contrary, large failure was observed for NSH which reached up to slope surface where tensile cut was also seen which increased with the time of excavation.

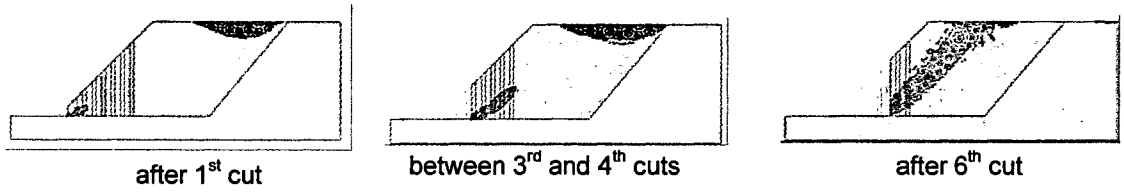

Fig. 8(a). Development of Plastic points and tension cut off points in NSL numerical model.

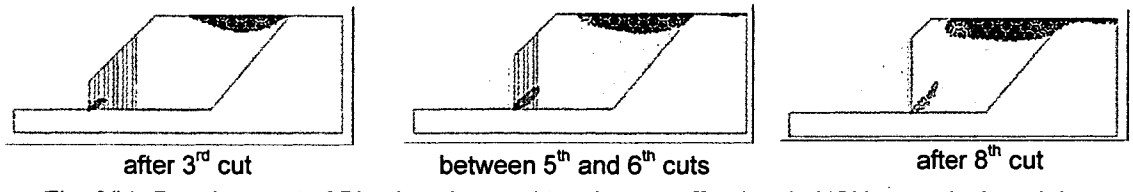

Fig. 8(b). Development of Plastic points and tension cut off points in NSH numerical model.

Figs. 9(a) and 9(b) show the vertical displacement calculated from the numerical analysis on the slope tope with the increase in the excavation steps. In the figures, the measurement positions from the slope top are also shown. Gradual increase in the vertical deformation from the start of the excavation could be seen for the both NSL and NSH numerical models. Although both figures show the similar trend of increment in the deformation, their increment amount is different, NSH showing higher deformation value than NSL.

4.4 Comparison of vertical displacements

In Fig. 10, vertical deformations either directly measured or indirectly estimated at 0.5m distance

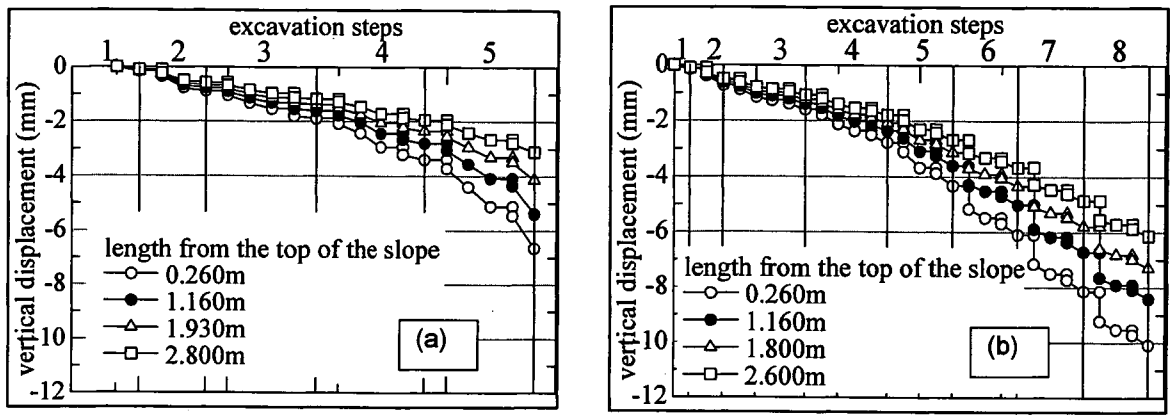

Fig. 9. Vertical displacement measured for (a) NSL and (b) NSH in the numerical analysis.

from the slope crest for field test, centrifuge test and numerical analysis are shown. In case of field (Fig. 10(a)), vertical displacement measured with laser beam-optical sensor which was placed exactly at 0.5m distance from the slope crest is shown. In case of centrifuge (Fig. 10 (b)), since the LVDTs were not set up at 0.5 m distance (in proto type scale), the average values between first two LVDTs nearer to the slope crest was estimated. Similarly, for the numerical analysis (Fig. 10(c)) also, average values for 0.5m distance was calculate. In each figure, vertical displacement after each step of excavation is shown. It is to be reminded here that the time difference of centrifuge excavation and other two cases were not same. Comparing the vertical displacements in three cases, it could be seen that the displacement value calculated in the numerical analysis was minimum; centrifuge model test giving the maximum value. Deformations were seen from the start of excavation steps in case of centrifuge and numerical analysis where as it was seen only after the 4th excavation step in case of field embankment. Although there is difference in the amount of displacement values, in overall, it could be said that their failure trend after 4th excavation step resembles with each other. Comparing the failure steps, it could be seen that failure occurred after 6th cut in both centrifuge and field embankment for NSL. But the failure step for NSH was after 6th cut for centrifuge and after 8th cut for field embankment.

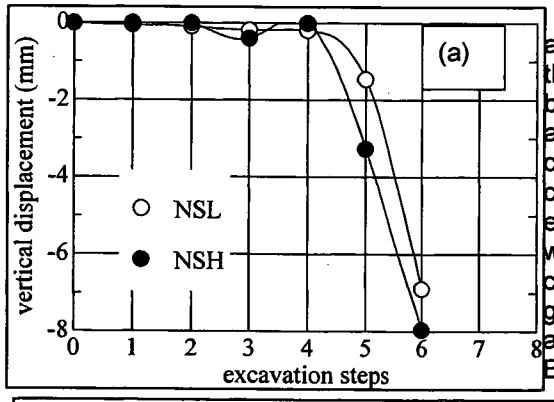

Difference in the failure steps and deformation amount in three cases might be due to the difference in their preparation, time allowed before the test and boundary conditions. In the field, three dimensional affect might be prominent along with the degree of compaction and grain size of the soil used for compaction might not uniform through out the embankment. Also, excavations of the embankments were conducted after few days of its construction. In case of centrifuge, friction between the sides of the glass pans and rubber membrane might have affected a lot. Soils passing through 2mm sieve were only used. Excavation tests were conducted immediately after its

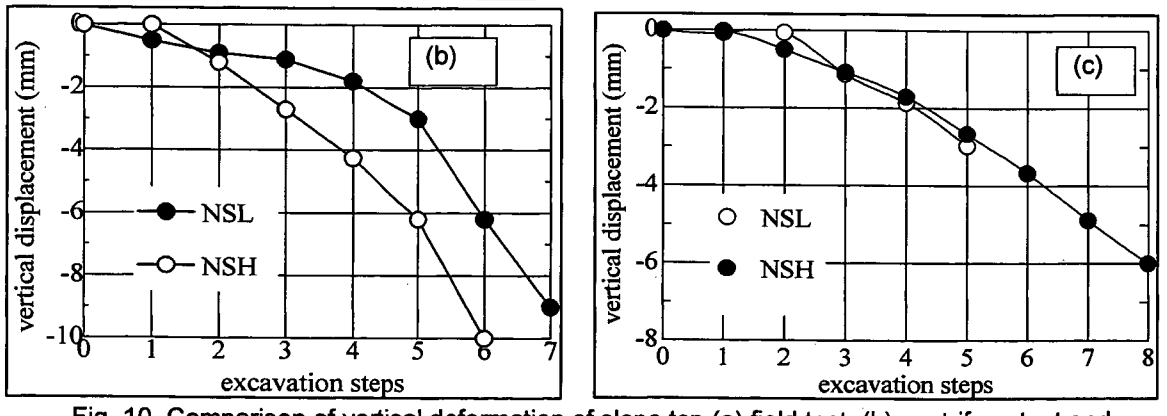

Fig. 10. Comparison of vertical deformation of slope top (a) field test, (b) centrifuge test and (c) numerical analysis.

preparation. Numerical analysis done here was only two dimensional. In addition, stiffness parameters for the analysis were only estimated values from N-values.

5. Conclusion

To clarify the failure mechanism of slope failure during the toe excavation, field embankment excavations, centrifuge in-flight excavations and numerical were carried out in this paper. Following conclusions were withdrawn:

1. From the numerical analysis, it could be said the loosely compacted NSL embankment failed due to spreading of plastic strain points from the toe towards the slope top. Whereas NSH embankment was failed due to development and increment of plastic strains at the toe and tension cut off points at the slope top, respectively. Similar failure patterns for NSL and NSH in the field were observed.

2. Although there are some differences in the amount vertical displacement, in all the excavation large and sharp increment in vertical deformation could be seen. Deformations measured with invar extension wire and laser beam-optical sensor in the field excavations showed almost same amount and similar trend of deformation with time. This shows the applicability of these instruments for the measurement of deformation at the slope crest.

3. In case of centrifuge excavations, LVDT set up closest to the slope crest showed the maximum value. This shows the best position for the measurement of deformation during the excavation.

6. Acknowledgement

This research is carried out under the Health and Labor Sciences Research Grants of Ministry of Health, Labor and Welfare. Authors would like to extend their thanks to Ms. Sumine Kusakabe and Mr. Takuma Koitabashi for their support in carrying out the tests and analyses.

7. References

[1] Tamrakar S.B., Toyosawa, Y., Itoh, K. & Timpong, S. (2006): "Comparison of failure heights during excavation of slope using In-flight excavator", International conference on Physical Modeling in Geotechnics, Physical Modelling in Geotechnics-6th ICPMG 2006, Ng, Zhang and Wang (eds),Vol. 1, pp. 385-390, ISBN 0-415-41586-1
[2] Tamrakar S.B., Toyosawa Y., Tanaka H. and Itoh K. (2006): Possibility of measurement of slope movement during the Sandy soil slope failure in centrifuge, Sea to Sky Geotechnique-2006, 59th Canadian Geotechnical Conference, pp. 351-358
[3] Saitoh A. et al. (2002): The field observation of the Slope with a new Inclination used for, Soils and Foundations, Japanese Geotechnical Society, Vol. 50, pp. 4-6.
[4] Tamate, S., Endo, A., Suemasa, N. and Katada, T. (2006); Monitoring the slope failure using the screw rod type bending sensor, 41st annual conference of Japan Geotechnical Society, JGS, pp. 2257-2258.
[5] Itoh, K., Toyosawa, Y. Takeyama, M. and Sano, T. (2006): The development of slope failure detection system using a laser beam and optical sensor, 41st annual conference of Japan Geotechnical Society, JGS, pp. 2251-2252.
[6] Horii, N., Itoh, K., Toyosawa, Y., Tamate, S. and Tamrakar, S.B. and Hashizume, H. (2006): Field test related to slope failure during slope cutting work (Part 1: Outline of field test), 41st annual conference of Japan Geotechnical Society, JGS, pp. 955-956.
[7] Horii N., Itoh K, Toyosawa Y., and Tamate S. (2006): Development of the NIIS Mark-II Geotechnical Centrifuge, International Conference on Physical Modelling in Geotechnics, Hongkong, pp. 141-146
[8] Toyosawa, Y., Horii, N., & Tamate, S. (1998): Deformation and failure behavior of anchored retaining wall induced by excessive excavation in centrifuge model tests, Research Reports of the National Institute of Industrial Safety, (NIIS-RR-97): 35-46.
[9] Geotechnical engineering memo, http://www.cive.gifu-u.ac.jp/lag/up3/Geotech_HW2004_No2.pdf.
[10] Okada, K., Sugiyama, T., Noghuchi, T and Muraishi, H. (1992): A correlation of soil strength between different sounding tests on embankment surface, Soils and Foundation, Vol. 40, No. 411, pp. 11-16.

The Nineteenth KKCNN Symposium on Civil Engineering
December 10-12, 2006, Kyoto, Japan

Observation of the Behavior of Soil Element behind Deep Diaphragm Wall by Triaxial Tests on Bangkok Clay

*Nghia Trong Le[1], Wanchai Teparaksa[2], Toshiyuki Mitachi[3] and Takayuki Kawaguchi[4]

ABSTRACT

Even a large area and deep excavation takes a long time and many steps to finish, the response of clay soil at the moment of excavation is usually considered as undrained. The simple linear elastic-perfectly plastic model with soil parameters s_u, E_u and ν is usually applied to predict the displacement of diaphragm wall (DW) during and immediately after finishing excavation. However, the collected data on the site showed that the displacement of the DW continued increasing both during the elapsed time without activity of excavation and after finishing excavation. The main purpose of this paper is to observe the creep behavior of soil elements behind DW with conditions of the undrained and drained unloading compression by triaxial tests. The soil sample is applied by the stresses same as the state of soil during excavation to determine its creep characteristics of both axial and lateral strain.

INTRODUCTION

The creep displacement is happened not only on the ground settlement of embankment but also on the lateral displacement of retaining wall. Especially, the large area of excavation is divided into many small zones that take a long elapsed time for concreting the basement floors or install the strut and anchor systems. During that time, the total stress condition of the soil behind the wall is almost unchanged; however, the observed lateral displacement of the retaining wall is non-stopping.

A movement of DW was observed at the BOT project, located on the Chao Praya River bank, Bangkok, which is consists of five underground basement floors with the total depth of excavation is 15.2 m. The area of excavation is larger than 10790 m^2, and was divided into many small zones for excavation. It took more than one year to finish all the excavation and top-down construction for the basement floors. The depth of excavation was stopped over at three main stages 2, 4 and 6 as in Fig. 1., and the depths are respectively 1.25 m, 8.1 m and 15.2 m. On those stages, there are the stop times of excavation to concrete the basement floors before continuing excavation deeper, and the displacement of DW is uninterrupted increase as in Fig. 2.

Many researchers have studied on creep behavior of the natural soil [1] but the creep behavior under unloading compression has not been considered up to this time. In this paper, a series of K_0 consolidated unloading compression triaxial test are carried out to observe the creep deformation of the soil sample behind the DW. To determine the lateral displacement of DW on the elapsed time excavation, we concern only on the deformation of the soil sample on the primary period with 24 hours maintaining the same situation of stresses. Moreover, the specimen is applied increasing steps of the deviator stress until reaching to rupture. The strain rate of both axial and lateral strain is determined versus time.

MATERIAL TESTED AND TESTING PROCEDURE

The undisturbed soil samples, 15 cm height and 7.5 cm in diameter, were taken from two 15.5 m depth boreholes of BOT project near the bank of Chao Praya River in Bangkok. The properties of those samples are shown in Fig. 3. Specimens, 10 cm height and 5 cm in diameter, were trimmed from those undisturbed samples and, after that, saturated under 15 kPa of cell pressure and 5 kPa of back pressure at the beginning and gradually increase to, finally, 200 kPa of back pressure and 210 kPa of cell pressure. Then, all the samples were consolidated automatically to obtain K_0 condition with the vertical effective stress equal to estimated overburden stress at the depth of each sample. The duration to stop the K_0 process, that finishes the primary consolidation, was determined based on the 3t method [2]. Finally, the samples were continued carrying out the following tests:
(1) CK_0UC (K_0 Consolidated Undrained Compression): the specimens were sheared with undrained condition as conventional triaxial compression test at 0.1 %/min of axial strain rate. The undrained shear strength (s_u) and undrained Young's modulus (E_u) at 0.01% of axial strain of the samples are shown in Fig. 3.

[1] *Graduate Student, Chulalongkorn University, Thailand*
[2] *Associate Professor D. Eng., Chulalongkorn University, Thailand*
[3] *Professor D. Eng., Hokkaido University, Japan*
[4] Associate Professor *D. Eng., Hakodate National College of Technology, Japan*

(2) CK_0DUC (Anisotropically Consolidated Drained Unloading Compression): after anisotropic consolidation to be K_0 condition, the specimens were swelled (unloading compression) by decreasing lateral stress step-by-step from K_0 to K_f values while the axial stress was maintained constant. Each value of lateral stress is kept for 24 hours. During that time, the cell pressure and axial load are controlled automatically to maintain the vertical and horizontal effective stresses unchanged. The valve of back pressure is opened for drained condition.

(3) CK_0UUC (Anisotropically Consolidated Undrained Unloading Compression): this test is the same as the test number (2); however, the valve of back pressure is closed for undrained condition.

It was only considered the influence of creep to displacement of DW on period of excavation; therefore, on the test (2) and (3), the maintenance time for each load step is only 24 hours. The temperature during carrying out the experiments was kept as constant to be 24 ± 1 ^{0}C to eliminate the influence of temperature as variable.

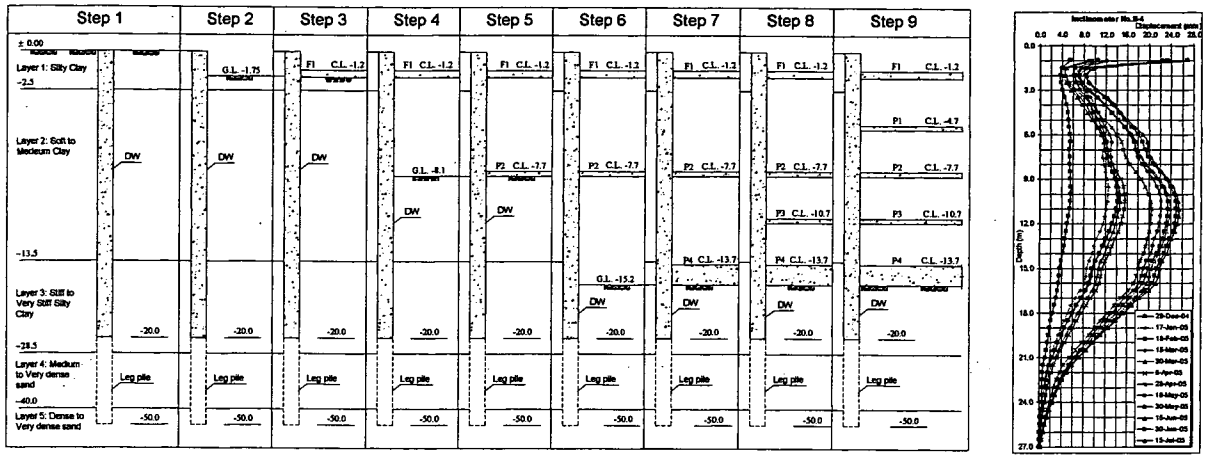

Fig. 1. Process of excavation of top-down construction and inclinometer data in BOT project

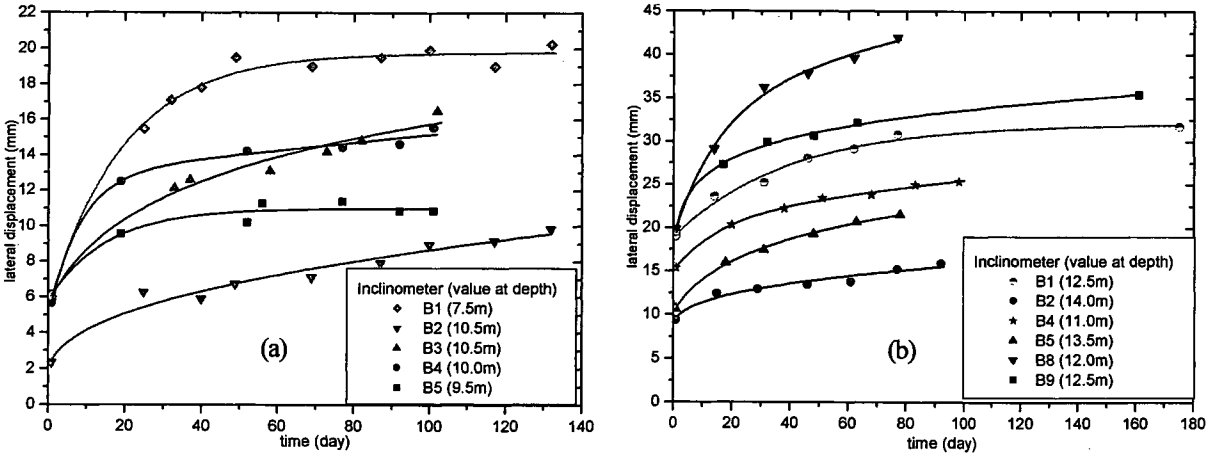

Fig. 2. Lateral displacement of diaphragm wall on the elapsed time excavated to (a) 8.1 m and (b) 15.2 m.

TEST RESULTS AND DISCUSSIONS

Many researches on soft Bangkok clay found out the values of the ratio E_u/s_u, because the main purpose is reduction the input parameter of elasto-perfectly plastic soil model for applying finite element analysis on the retaining wall structure. Some values of this ratio were predicted by back analysis of the lateral displacement of the wall such as that ratio varies of 200~500 (Bowels, 1988) and 280~350 for soft clay, and 1200~1600 for stiff clay (Hock, 1997), 500 and 2000 for soft Bangkok clay and stiff clay (W. Teparaksa et al., 1999). Actually, the ratio Eu/s_u is a function of many variables, e.g., the strain level (Mair, 1993), plasticity index and OCR (Duncan and Buchigani, 1976). As shown in Fig. 4b, the undrained shear strength absolutely depends on the strain value at which the ratio $(\sigma_1 - \sigma_3)/2\sigma'_{v0}$ reaches to peak. Base on relationship q - ε_a of the CK_0UC tests, the ratio E_u/s_u, calculated with values of s_u at peak and undrained Young modulus of lesser than 0.01% axial strain $E_{u(0.01\%)}$, gets high from 1100 to 1300 for weathered clay layer upper 4 m depth and 600 to 800 for normal soft soil layer as shown in Fig. 3. In addition, the undrained shear strength of the CK_0UC tests is approximate to the values of field vane-shear tests ($s_{u(FVS)}$ – in Fig. 3) ; therefore, the E_u values at a small strain ($\varepsilon_a \leq 0.01$ %) could be estimated from $s_{u(FVS)}$ instead of undrained shear strength of unconfined compression test (UC).

The ratio $(\sigma_1 - \sigma_3)/2\sigma'_{v0}$ of the samples more than 8 m depth, as shown in Fig. 4b, are lesser than 0.45, except the sample of CK_0UUC test, which behaves like lightly overconsolidated clay. In addition, these ratio of CK_0DUC test is smaller than CK_0UC test's. It could be explained based on early concept of Hvorslev that the shear strength is composed of an effective

friction increasing linearly with the effective stress and an effective cohesion. The cohesion component is mobilized with a small strain and will cause a gradual transfer of shear stresses to the more stable frictional contact points (Schmertmann and Osterberg, 1961). In case of CK_0DUC test, the load is applied discontinuously by keeping the same state of effective stresses for 24 hours. Therefore, the cohesion component is not mobilized completely while the frictional strength is quickly mobilized by drained condition. As the result, the shear strength of clay of CK_0DUC test is only equal to the residual strength of CK_0UC test; however, approximately equal value of critical state stress ratio M is obtained by the two kind of tests (Fig. 4a).

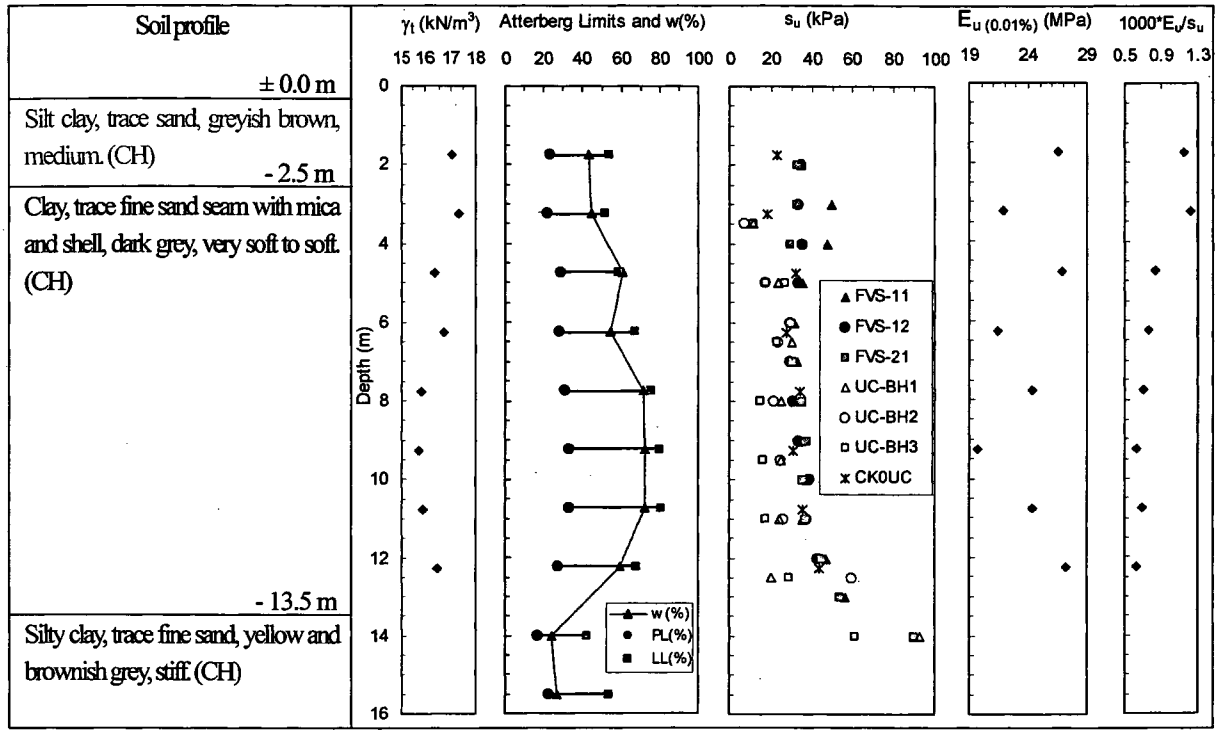

Fig. 3. Geotechnical properties at BOT project.

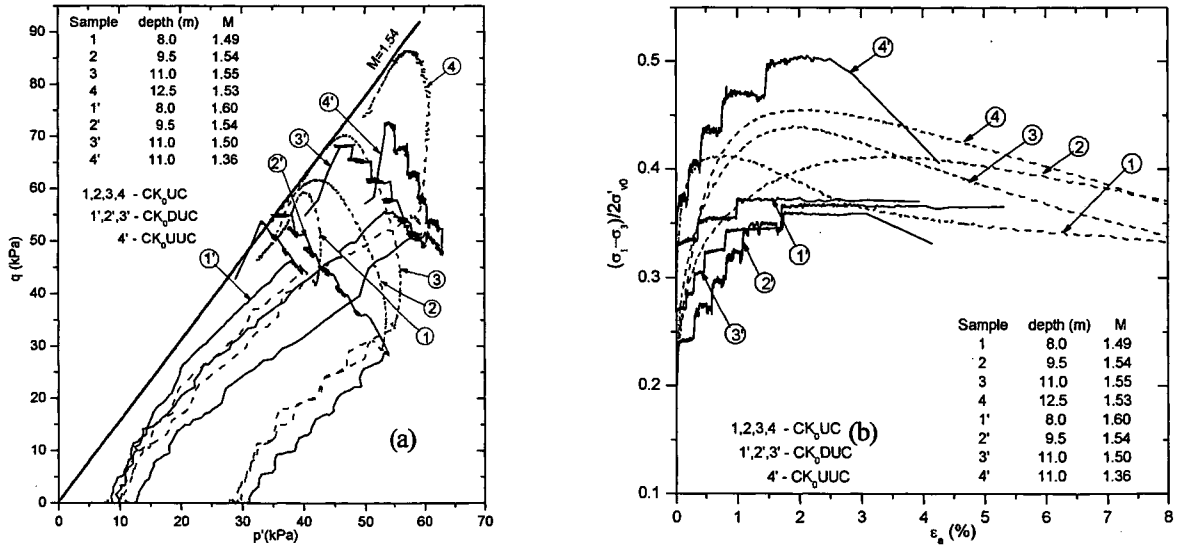

Fig. 4. Chart (a) q-ε_a and (b) p'-q of CK_0UC, CK_0DUC and CK_0UUC tests.

The strain rate curves are derivative of strain rate functions, which are approximately determined by the exponential function of time. These curves immediately reached to the large value after unloading and reduced virtually linear versus time as shown in Fig. 5b and Fig. 6b. The coefficient of deformation with time (C_α) of clay is usually determined from vertical strain of oedometer test or the volumetric strain of the isotropic consolidation test. In this study, we simulate the deformation condition of the backfill of DW by unloading compression test and C_α for horizontal and vertical strain during excavation can be calculated with the equation $\dot{\varepsilon} = C_\alpha / t(1 + e_0)$ [3]. It can be seen from Fig. 5b and Fig. 6b that C_α as well as strain rate depend on the deviator stress level, time and the direction of deformation.

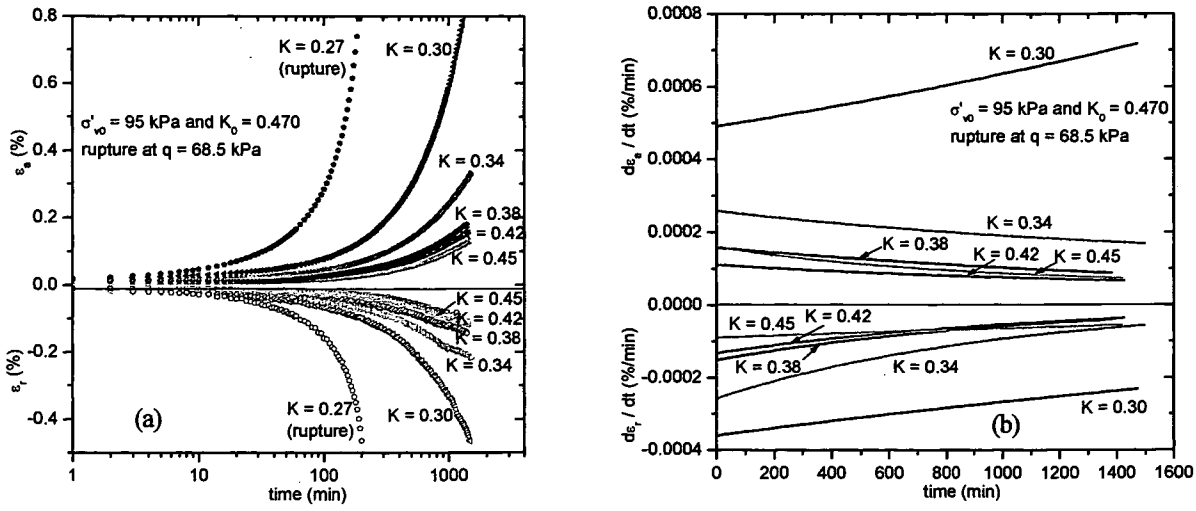

Fig. 5. Strain rate of soil sample at depth 11.0 m under CK_0DUC test.

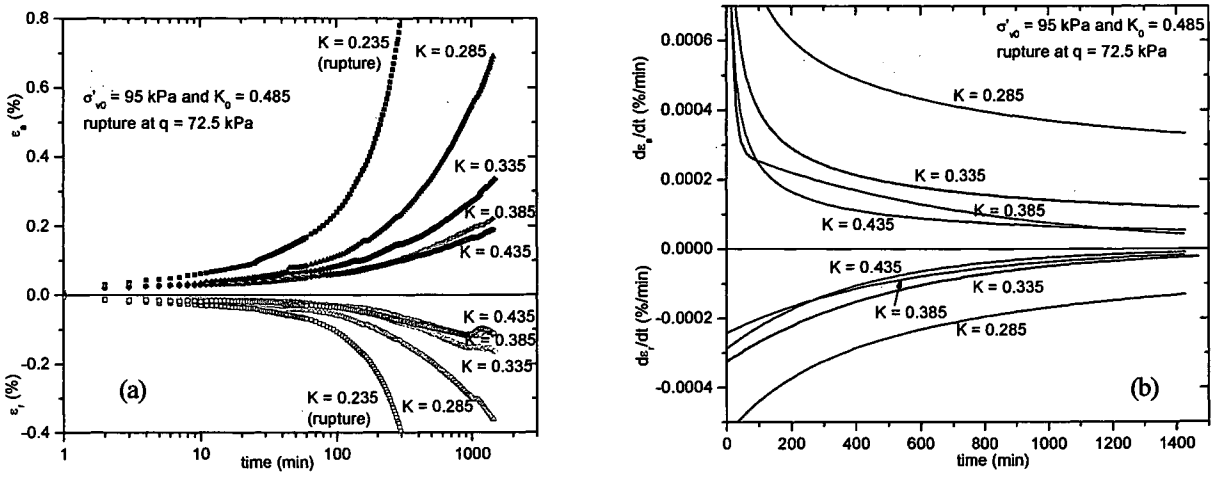

Fig. 6. Strain rate of soil sample at depth 11.0 m under CK_0UUC test.

CONCLUSIONS

Based on the field vane-shear test and the series of triaxial tests, the following conclusions can be darwn.

1. To predict the initial lateral displacement of DW by using elasto-perfectly plastic model, the undrained Young's modulus of soil could be determined based on the ratio $s_u/E_{u(0.01\%)}$ and undrained shear strength at peak of CK_0UC test or field vane-shear test. For the Bangkok clay at BOT project, the ratio $s_u/E_{u(0.01\%)}$ is from 1100 to 1300 for weathered clay layer upper 4 m depth and 600 to 800 for soft soil layer deeper than 4 m. It should be taken the residual shear strength of clay from the CK_0UC test for secure the stability of DW in the case the duration of excavation takes a long time.

2. According to the results obtained from CK_0DUC and CK_0UUC tests, the coefficient of deformation with time (C_α) as well as strain rate depends not only on the deviator stress level, elapsed time and drainage condition but also on the direction of deformation.

ACKNOWLEDGEMENTS

The triaxial tests on this paper were carried out at Soil Mechanics Laboratory of Hokkaido University and Hakodate National College of Technology. Thanks to Japan International Cooperation Agency (JICA) support financial for this research.

REFERENCES

[1] Mitchell, J. K. and Soga, K., "Fundamentals of Soil Behavior", Chapter 12, 2005

[2] "Standards of Japanese Geotechnical Society for Laboratory Shear Test (English Version)", The Japanese Geotechnical Society, May 1999.

[3] Tavenas, F., Leroueil, S., LaRochelle, P., and Roy, M. 1978. "Creep behaviour of an undisturbed lightly overconsolidated clay". Canadian Geotechnical Journal, Vol. 15, pp. 402–423.

Development of Tilt-sensor and possibility of measurement of failure trend just before the failure

Monitoring on site/measurement, Slope, Excavation

Institute of Industrial Safety Int. member O Surendra B. Tamrakar
Yasuo Toyosawa and Itoh Kazuya
Akebono Brake Industry Co. Ltd.. Kunimi Takashi
Nishijo Atsushi and Okubo Satomi

1. Introduction

Sudden failure of slope during or just after the excavation works causes many accidents which sometimes takes the lives of workers. Lives of the workers and property could be saved if early predictions of failure could be made. Many instruments have been developed to measure the movement of slope just before the failure. But most of them are either difficult to set up in the real field or are expensive to opt. Here, early response of slope failure just before the failure during the excavation is tried to measure using a tilt-sensor. Model slope was prepared in the field by lightly compacting Narita sand and excavation at toe of the slope was continued until slope was failed. Tilting angle (movement) of tilt-sensor was measured through out the excavation test until the failure occurred. Sharp movement of tilt-sensor just before was observed. This shows the possible use of tilt-sensor in the excavation field to predict the failure in advance.

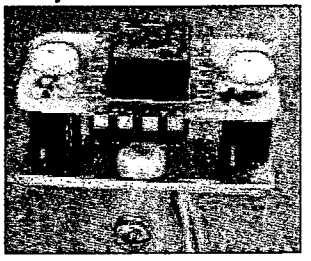

Photo 1 Tilt-sensor with two Accelerometers.

2. Tilt-sensor

Tilt-sensor mentioned here consists of highly sensitive accelerometers which are made by anodic bonding of three layers of Silicon (Two fixed and one movable) and glass. In principle, capacitance between the movable and fixed electrodes changes when the center mass of sensor inclines, thereby, changing the gap between the electrodes. By converting the capacitance into voltage and by calibrating tilt angle and voltage later on, one could measure the tilt angle (degree of movement)[1]. Thus, during the test, only output voltage is measured. Generally, two accelerometers are attached into one tilt-sensor so that the tilting angles along X and Y directions could be measured. Tilt-sensors used here could measure the angles in the range of ±20° with the sensitivity of 100mV/deg. Since temperature variation affects the measurement of angles, sometimes, one more accelerometer is attached to tilt-sensor, as accelerometers could also be used as a thermal sensor with thermal sensitivity of 10mV/°C. Accelerometers are set up on the base plate which is further supported by flat or tubular pipe. Tilt-sensor shown in Photo 1 consists of two accelerometers (for X and Y directions) whereas tilt-sensors shown in Photo 2 comprise of three accelerometers (for X, Y directions and temperature). Direction of movement of tilt-sensor is shown in Fig. 1. Here, X represents the movement normal to the slope surface, i.e. inward or outward movements from the slope surface; inward being negative and outward being positive. Similarly, Y represents the movement along the slope surface, i.e. right or left side of the slope. Movement towards right side is considered as positive and that on left side as negative. In this research, model slope is made at the field and two types of tilt-sensor are used; Small Size Compact (SSC) and Stand Alone (SA). First type is small in size and light to handle and easy to set up. While second type is little bigger and need heavy base support.

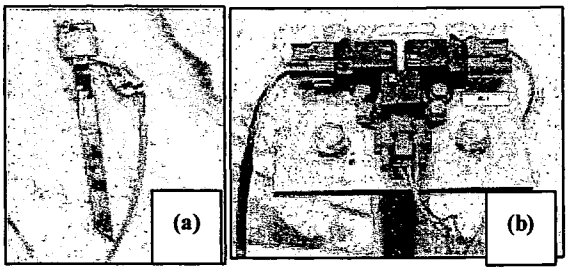

Photo 2 (a) Small Size Compact (SSC) Tilt-sensor and (b) Stand Alone Tilt-sensor (SA)

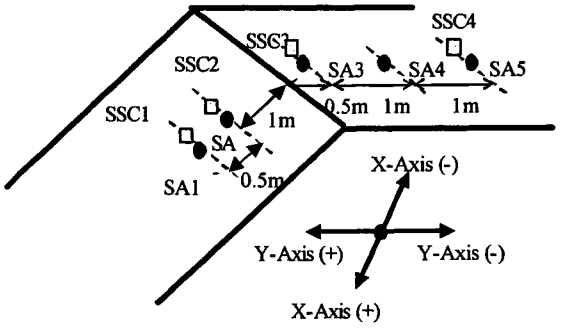

Fig. 1 General layout of Tilt-sensors set up model

3 Field Test

In this research, model excavation test in the field was carried out. Model slope was prepared from Narita sand (wet density, ρ_t=1.67 g/cm^3 and water content, w=26.5%). The height, width and slope angle of the model slope were 5m, 3.5m and 45°,

Development of Tilt-sensor and possibility of measurement of failure trend just before the failure
Surendra B. TAMRAKAR, Yasuo TOYOSAWA, Kazuya ITOH (National Institute of Industrial Safety),
Kunimi TAKASHI, Nishijo ATSUSHI and Okubo SATOMI (Akebono Brake Industry Co. Ltd.)

respectively. Both types of tilt-sensors; SSC and SA were setup on the slope surface and slope top as shown in Fig. 1 where distances and numbering of sensors are also done. There are four SSC (SSC1, SSC2, SSC3 and SSC4) and five SA (SA1, SA2, SA3, SA4 and SA5) tilt-sensors. The slope surface is divided into 10 equal widths so that each excavation (cut) width is equal to 0.5m. Excavation is started from the toe of the slope, vertically downward using a backhoe. Therefore, the height of excavation in each cut increases by 0.5 m. Five minutes waiting time was allowed after each cut. Cutting of slope was done until the slope failure occurred. Here, total of 6 cuts were done. Some partial failure within the slope was observed after 5th cut. But the final large failure was observed after 6th cut, failure reaching up to the slope crest.

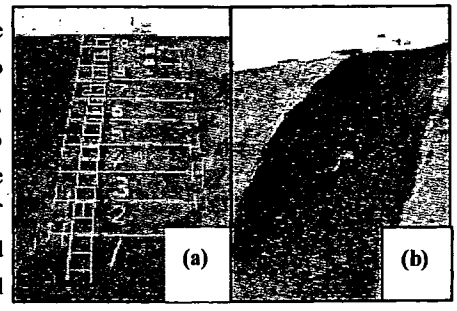

Photo. 3 (a) Before cut and (b) after failure

3. Test Results

Photo 3 shows the model slope before the starting of the cut and after the failure. Cracks were also seen before failure on the slope top. Figures 2 and 3 show the movement of SSC and SA tilt-sensors measured along X and Y directions. Movement of the whole slope could be made by comparing the X and Y movements. In the figures, solid vertical lines represent the number of cut and dashed line in between the solid lines represents occurrence of partial failure whereas the dashed line at the end represents the final failure. Although it is difficult to see the amount of movement for the first few cuts, increment in the slope movement with the progress of cut could be seen in all the sensors. In all the figures, sharp increment in the movement after 5th and 6th cuts could be seen. Partial failure was observed after 5th cut (at 48 min.) and final large failure was observed after 6th cut. Just before the occurrence of both failures, sharp increment in the tilt angle could be seen in all the cases, especially SSC 1, 2 and SA 1, 3. Since the trend of failure pattern could be clearly measured using these tilt-sensors, practical application of these sensors in the real excavation field is possible. Comparing the ranges of movements (tilt angle) measured by SSC and SA placed at the same positions, it was found that their difference is very less which shows that both types of tilt-sensors are equally applicable in the field.

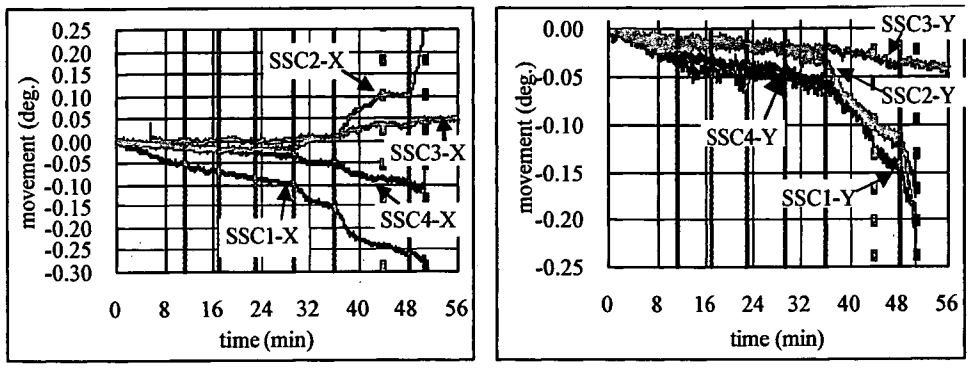

Fig. 2 Movement of slope surface and slope top measured from Small Size Compact Tilt-sensor

4. Conclusions

(1) Both types of tilt-sensors could measure the slope movement during the excavation. In addition, prominent and sharp movement of the slopes just before the failure could also be measured which shows the possible application of these tilt-sensors in the slope excavating field. (2) Measured amount of movement of tilt angle at the same position by SSC and SA tilt-sensors are almost same. This suggests that both types of tilt sensors could be used with equal preference.

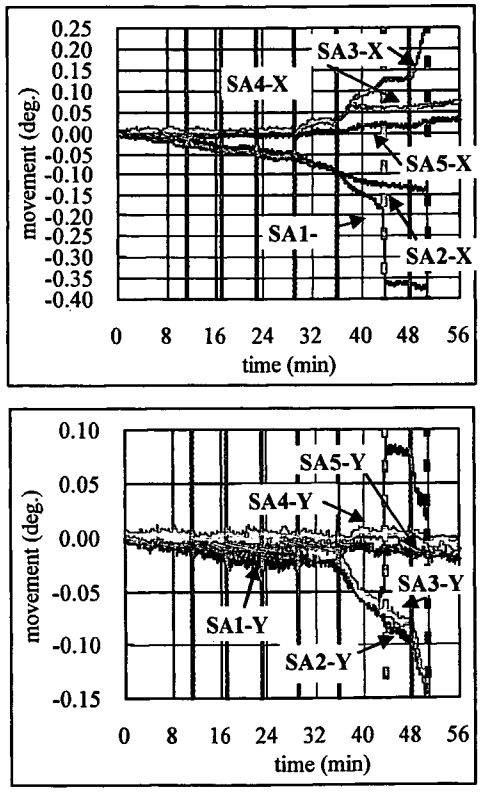

Fig. 3 Movement of slope surface and slope top measured from Stand Alone Tilt-sensor

5. Acknowledgement

This work is partially carried out under the Health and Labor Sciences Research Grants of Ministry of Health, Labor and Welfare.

References

Takemoto, M., Satou A., Matsuyma H., Ogata K., Kunimi T., Ito S. and Nezu M, 2001, "*Development of new In-place inclinometer in bore using accelerate sensor*", 36th Annual meeting of Japanese Geotechnical Society, pp. 179~180 (in Japanese).

Comparison of slope failure trend just before failure in the field using newly developed tilt-sensor

Japan National Institute of Occupations Safety and Health Regular member O Tamrakar S. B.
Japan National Institute of Occupations Safety and Health Regular member Toyosawa Y. and Itoh K.
Akebono Brake Industry Co. Ltd. Non-member Kunimi T., Nishijyo A. and Okubo T.

1. Introduction

Tamrakar et al. (2006) have developed a new type of tilt-sensor which could be used to measure the movement of the slope just before the failure in terms of tilting angle. They had tested its application in the field with Narita sand embankment model using Small Size Compact (SSC) and large size Stand Alone (SA) type tilt-sensors. In this report, comparison of tilt angle measured from SSC and SA type Tilt-sensors for two different types of soil embankments (Narita sand and Kanto loam) are made and their failure pattern are discussed.

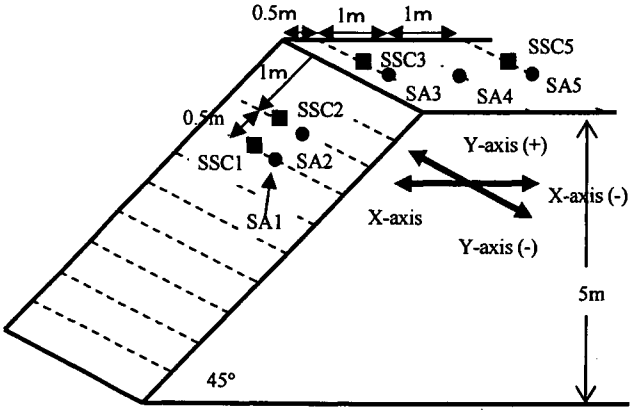

Fig. 1 Layout of tilt-sensors set up

2. Tilt- sensor and Field Test

Directions of movement of tilt-sensor (Tamrakar et. al, 2006) are shown in Fig. 1 and Photo 1. Four SSC (SSC1, SSC2, SSC3 and SSC5) and five SA (SA1, SA2, SA3 SA4 and SA5) tilt-sensors were set up on the slope surface and slope top (Fig. 1). Water content and wet density of Narita sand slope model and Kanto loam slope model obtained from sand replacement technique in the field were 1.74g/cm^3 and 29.3% and 1.18g/cm^3 and w=111.3%, respectively. Each model slope is of 5m height, 3.5 width and 45 degree slope angle. Slope surface was divided into 10 equal widths, each with 0.5 m. Excavation is started from the toe of the slope, vertically downward using a backhoe. Five minutes interval was allowed after each cut to see the failure trend. Cutting of slope was continued until the slope failure occurred. In case of Narita sand total of 6 cuts were made. Some partial failure within the slope was observed after the 5th cut. But the final large failure was occurred after 6th cut (around 51 min. elapsed time) which reached up to the slope crest. For Kanto loam, altogether 9 cuts were made. First partial failure was occurred after 8 cut (78 min. elapse time) at the right side of the slope (right wall). Large change in tilt angle could during this partial failure was stopped around 88 min. Further excavation on the left side of the slope was made so that final failure was occurred which reached up to SA3 (SSC3) position on the slope crest.

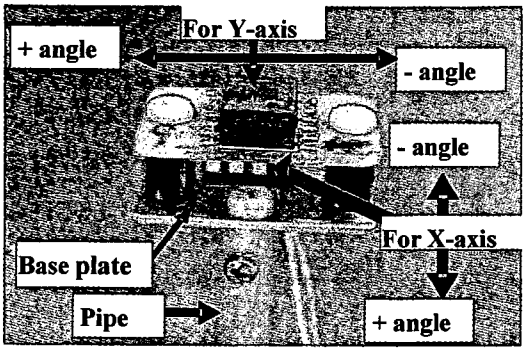

Photo 1 SSC-tilt-sensor

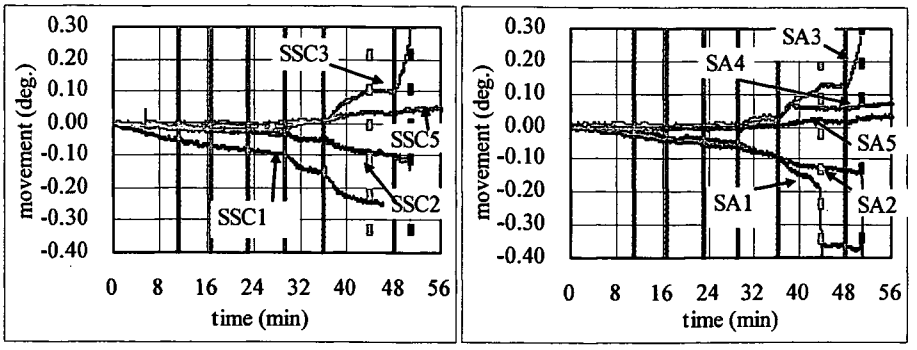

Fig. 2 Movements measured from SSC and SA Tilt-sensors (X-axis) for Narita sand

Keywords: **Monitoring on site/measurement, Slope, Excavation**

National Institute of Industrial Safety, JNIOSH, Construction Safety Division,
1-4-6 Umezono, Kiyose-Shi, Tokyo-204-0024. Tel: 042-491-4512, Fax: 042-494-6214, Email:tamrakar@s.jniosh.go.jp

3. Test Results

Movement of slope with SSC and SA tilt-sensors along X-direction for Narita sand and Kanto loam are shown in Figs. 2 and 3 (only X-direction is shown). Solid thick vertical lines in the graph show the end of excavation steps. Dotted lines in between these lines show the occurrence of partial failure where as the last thick dotted line shows occurrence of final failure. Sudden change in the tilt angles was seen just before the partial and final failures in both types of tilt–sensors. Kanto loam showed larger movement and took longer time to fail than that by Narita sand despite of wet density of Narita sand being higher than that of Kanto loam. Comparing the movements of SSC and SA for each soil, similar pattern of failure movement could be seen. In case Narita sand, SSC1, SSC2, SA1 and SA2 showed negative values while SSC3, SSC5, SA3, SA4 and SA5 showed positive value. Negative values shows the backward and downward movement of slope while the upper tilt sensors placed on the slope top showed the forward and downward movement of slope (Fig. 4(a). This shows the movement of slope during partial and final failure in different directions. In case of Kanto loam also similar movements of SSA and SC tilt-sensors were seen. Here, all the sensors moved forward and downward, showing partial and final movement taking in the same direction (Fig. 4(b)). Change in the tilt angle for each tilt-sensor along X-direction at particular elapsed time for each soil type is shown in Table 1. Comparing the amount of change in the tilt angle, it was seen that both types of tilt-sensors show almost same values except SSC2, SA2, SSC5 and SA5. This shows the application of both types of tilt-sensors with equal efficiency in the field.

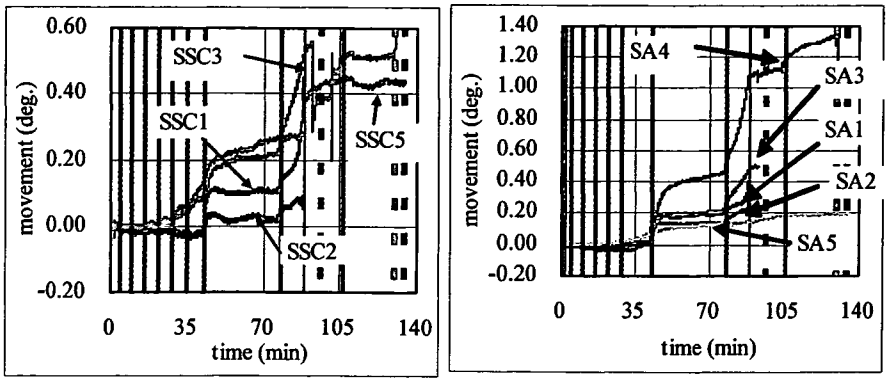

Fig. 3 Movements measured from SSC and SA Tilt-sensor (X-axis) for Kanto loam

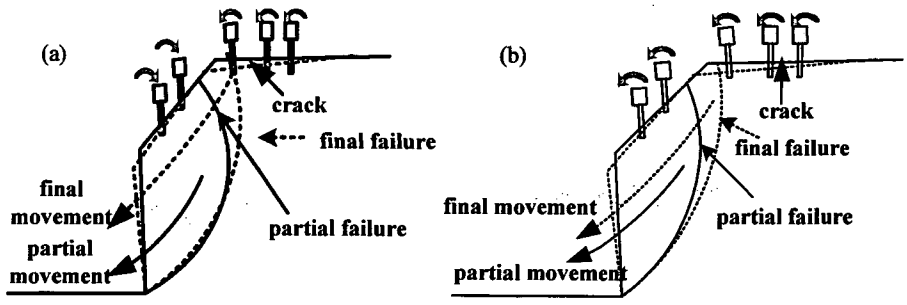

Fig. 4 Failure pattern in two types of soil models (a) Narita sand and (b) Kanto loam

Table 1 Comparison of tilt-angles measured

Narita sand (around 51 min. elapsed time)					
tilt-angle (X-axis)	1	2	3	4	5
SSC	-0.275	-0.11	0.25	-	0.025
SA	-0.300	-0.15	0.25	0.06	0.025
Kanto loam (around 88 min. elapsed time)					
tilt-angle (X-axis)	1	2	3	4	5
SSC	0.50	0.08	0.54	-	0.400
SA	0.50	0.30	0.50	1.08	0.150

4. Conclusions

1). Sudden movement just before failure could be seen in both types of tilt-sensors. Both SSC and SA tilt-sensors show almost same pattern and same amount of movement for particular soil model. This shows the application of both types of tilt-sensors in the field with equal efficiency. 2). Failure pattern of different soil could be measured with this new type of tilt-sensor. In case of Narita sand, partial and final failure directions are different whereas for Kanto loam, they are same.

Acknowledgement

This work is partially carried out under the Health and Labor Sciences Research Grants of Ministry of Health, Labor and Welfare.

References

Tamrakar, S.B., Toyosawa, Y., Itho, K., Kunimi T., Nishijo A. and Okubo S., 2006, "Development of Tilt-sensor and possibility of measurement of failure trend just before the failure", 41th Annual meeting of Japanese Geotechnical Society (under print)

Development of Tilt-sensor for advance prediction of failure and its applicability in the field excavation

Ọ Tamrakar S.B., Toyosawa Y. and Itoh K. (Japan National Institute of Occupational Safety and Health)

1. Introduction

Main purpose of this report is to develop some kinds of measuring instrument, which could measure the slope movement in the real excavating field with which the pattern of failure could be predicted in advance. In this report, in reference to the tilt sensors developed by Tamrakar et al. (2005), two new types; small size compact (SSC) and large size stand alone (SA) were developed and their applicability in the real excavating field was explained. Four types of model slopes were prepared from two types of soils; Narita sand and Kanto loam by compacting each type to Low (L) and High (H) density. Excavation at the toe of the slope was continued at certain interval until the failure occurred. Both types of tilt sensors were set up both on the slope top and slope surface and measurement was done until the failure. Sharp movement of tilt sensor just before the failure was observed for each slope. Finally, tilt angles measured from above tilt sensors during the excavation of Narita sand (L and H) and Kanto loam (L and H) embankments were made. Also, failure patterns were discussed.

2. Tilt sensor

Tilt-sensor used here consists of highly sensitive accelerometers which could measure the tilting angle in the range of ±20° with the sensitivity of 100mV/deg and have thermal sensitivity of 10mV/°C. Both positive and negative angles along both X and Y directions could be measured as shown in Photo 1. Depending upon the requirement of measurement of tilting angle (X and Y directions) and temperature variation, one set of tilt sensor is provided with one, two or three accelerometers. Photo 1 shows the general outline of the tilt sensor used by Tamrakar et. al (2005). In Photo 2, two new tilt sensors; small size compact (SSC) and stand alone (SA) developed to use in the excavation field are shown. It is to be mentioned that SSC is small, simple and compact whereas SA is large and robust. Inner structure of SSC tilt sensor is similar to that shown in Photo 1 which comprises of two accelerometers (X and Y directions). SA tilt sensor comprises of three accelerometers (X, Y directions and temperature). In case of SSC, accelerometers are placed in layers above the base plate whereas in case of SA, accelerometers are directly placed on the base plate. Base plates of SSC and SA sensors are further supported by either flat plate (Photo 2(a)) or tubular pipe (Photo 2(b)). Both of these sensors are directly set up on the slope top and slope surface.

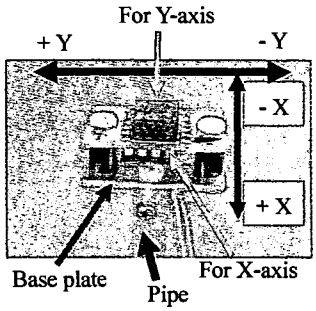

Photo 1 Tilt sensor.

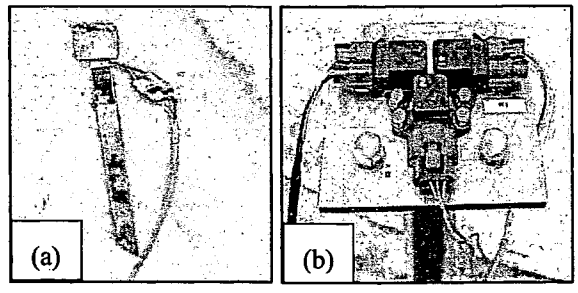

Photo 2 (a) SSC and (b) SA tilt sensors.

3 Tilt sensors set up and Field Test

Four model slopes were prepared from Narita sand and Kanto loam by compaction them with a small size bull dozer. Properties of each soil are shown in Table 1. For each type of soil, two model slopes with two types of densities; high (H) and low (L) were prepared. The height, width and slope angle of the model slope were 5m, 3.5m and 45°, respectively. At 2.5m and 5 m

height, density and water content were measured by two methods; Sand replacement and Core cutter. Average unit weight and water content for each model slopes are shown in Table 2.

Table 1. Properties of soil specimens.

	Narita Sand	Kanto loam
Unit weight of soil solid (kN/m^3)	26.12	27.13
Liquid limit, w_L (%)		129.3
Plastic limit, w_P (%)		91.2
Plasticity index, Ip		38.1
0.075x10^{-3}~2x10^{-3}m (%)	77.5	11.5
0.005x10^{-3}~0.075x10^{-3}m (%)	12.7	54.7
<0.005x10^{-3}m (%)	9.8	33.8
Avg. particle size, D_{50} (x10^{-3}m)	0.1909	0.0119
Soil classification	SF	VH_2-S

Table 2. Density and water content

Method	Type	Narita Sand		Kanto loam	
		w	unit wt.	w	unit wt.
		(%)	(kN/m^3)	(%)	(kN/m^3)
Sand replacement	Low	29.35	16.4	116.35	10.56
	High	27.45	17.09	111.25	11.62
Core cutter	Low	28.75	15.03	116.4	11.33
	High	28.75	16.16	112.6	11.65

Four SSC (SSC1, SSC2, SSC3 and SSC5) and five SA (SA1, SA2, SA3, SA4 and SA5) type tilt sensors were set up both on the slope and slope top as shown in Fig. 1. Slope surface was divided into 10 equal widths and excavation was started from the toe of the slope, vertically downward using a backhoe. Height and width of each cut were therefore change by 0.5m. About 5 minutes waiting time was allowed between each cut. Toe excavation was continued until full failure of the slope was occurred. Directions of movement of tilt sensor on the model slope are also shown in Fig. 1.

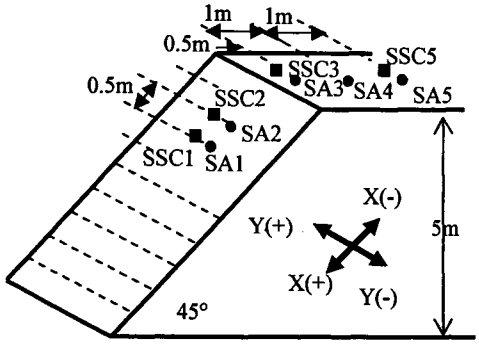

Fig. 1 Layout of slope and tilt sensor set.

In case of Narita sand (L) total of 6 cuts were made. Partial failure was observed after the 5th cut with longer waiting interval. Final large failure was seen after 6th cut at around 40.5 min. elapsed time. Similarly, for Narita sand (H), total of 6 cuts were made and here also, partial failure was observed after 5 cut. But the final failure was observed after 6th cut at around 51 min. elapsed time.

For Kanto loam (L), large partial failure within the slope was seen after 7th cut where SSC1, SSC2, SA1 and SA2 measurements became discontinuous, showing the partial failure reaching around those positions. Then 3 under-cuttings from 51~52.2 minutes were made to see the failure pattern. Movement of the crest of the slope was seen from SSC3 and SA3 tilt sensors with continuous increase in tilting angle measurement and it stopped at around 70 min. elapsed time. In case of Kanto loam (H), total of 9 cuts were made. First partial failure took place after 8 cut at the right side of the slope (right wall). Large change in tilt angle was observed during this partial failure which stopped at around 88 min. elapsed time. Further excavation on the left side of the slope was made and final failure was occurred around 135 min. elapsed time where the failure reached up to SA3 (SSC3) position on the slope crest. During the excavations, tensile cracks were appeared on the slope top in all the cases.

3. Test Results

In this report movements of SSC and SA tilt sensors along the X-direction placed on the slope surface and slope top are only shown. In all the figures, solid lines represent the end excavation for each step. Dotted line at the end shows the final failure time whereas those in between show the occurrance of partial failure except those dotted lines around 51~52.2 min. of Kanto loam (L) which were the under-cutting steps.

Figures 2 and 3 show the movement of SA and SSC tilt sensors measured along X-direction for Narita sand (L). Although it is difficult to see the amount of

movement for the first few cuts, increment in the slope movement with the progress of cut could be seen in all the sensors. Sudden increment in tilt angle measurement could be seen after 5 and 6 cuts. Comparing the movement of SA and SSC placed at the

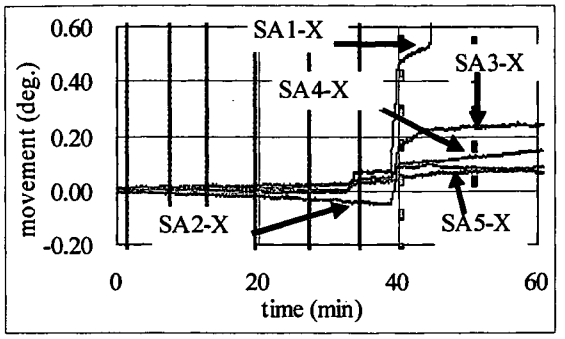

Fig. 2 Movement of SA for Narita sand (L).

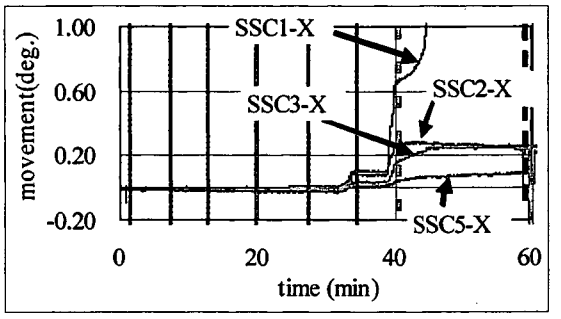

Fig. 3 Movement of SSC for Narita sand (L).

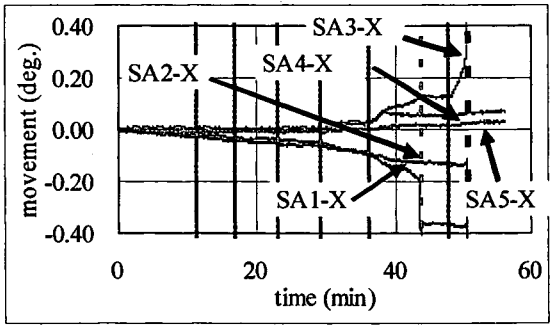

Fig. 4 Movement of SA for Narita sand (H).

same position, similar trend of movements could be seen. Here, all the tilt sensors moved along the positive X-direction only. Although, movements of SA and SSC along the Y-direction were not shown here, all the Y-direction movements were in the negative direction. This shows the movement of whole the slope in the front and left side of the slope face.

In Fig. 4, movements of SA tilt sensors for Narita sand (H) are shown. Here also, sudden increment in the tilt angle was seen after 5 and 6 cuts. Partial failure was stopped after 44 min. elapsed time and then final failure of whole slope took place at 51 min. elapsed time. In contrary to those of Narita sand (L), here all the tilt sensors placed on the slope surface moved in opposite direction to those placed on the slope top. Movements of SSC tilt sensor along Y-direction were negative (not shown). This shows the failure of slope for Narita sand (H) towards the left side of slope face by overturning of upper section of slope (slope crest).

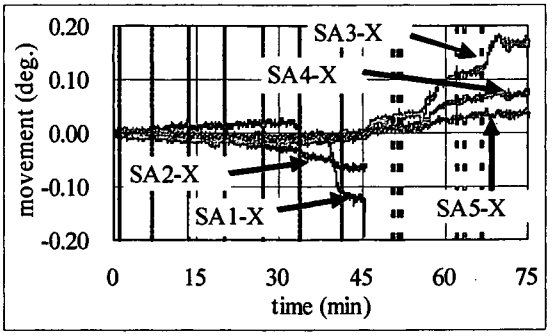

Fig. 5 Movement of SA for Kanto loam (L).

Figure 5 show the movements of SA tilt sensors along X direction for Kanto loam (L). SA1 and SA2 tilt sensors placed on the slope surface were out of order after 7th cut. Increment in the slope sensors took place after 3 under-cuttings made on the toe portion of slope. With partial failure, increment on the tilt sensor movement could be seen. Slope top tilt sensors showed positive X-direction. Movements of SSC tilt sensors (not shown) also showed the similar trend of movement as those by SA tilt sensors. Almost no movement was seen along Y-direction for all tilt sensors. Since the movement of tilt sensors placed on the slope surface could not be used after 7th cut, it is little difficult to trace the failure pattern of whole slope in this case.

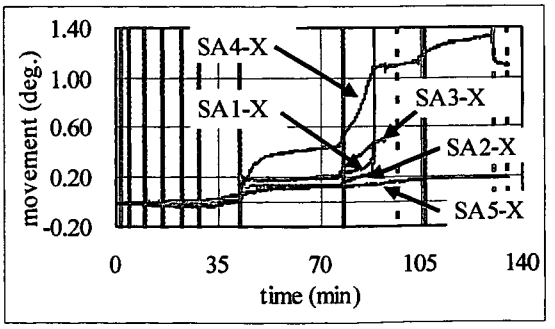

Fig. 6 Movement of SA for Kanto loam (H).

Movements of SA tilt sensors along X-direction for Kanto loam (H) are shown in Fig. 6. Sudden increment in the tilt angle was seen after 7th, 8th and 9th cut. After 7th and 8th cuts, two partial failures were observed. Positive movements along X-directions were seen for all the SA sensors. No movement along the Y-direction was found (not shown). Similar movement along both directions for SSC tilt sensors were found (not shown). This shows the movement of whole slope in the forward and outward from the slope face. This means that whole the slope during failure moved outward and downward from the slope face.

As explained in above, from the X and Y direction movements of tilt sensors, it is possible to predict the failure pattern of slope. In Fig. 7, failure pattern for Narita sand (H) and Kanto loam (H) are shown along with the direction of movement of tilt sensors placed on the slope surface and slope top. Changes in the tilt angle for each SA and SSC tilt sensor along X-direction at particular elapsed time for Narita sand (H) and Kanto loam (H) are shown in Table 1. By comparing the amount of change in the tilt angle, it was seen that Kanto loam (H) showed larger movement and took longer time to fail than that by Narita sand (H) despite

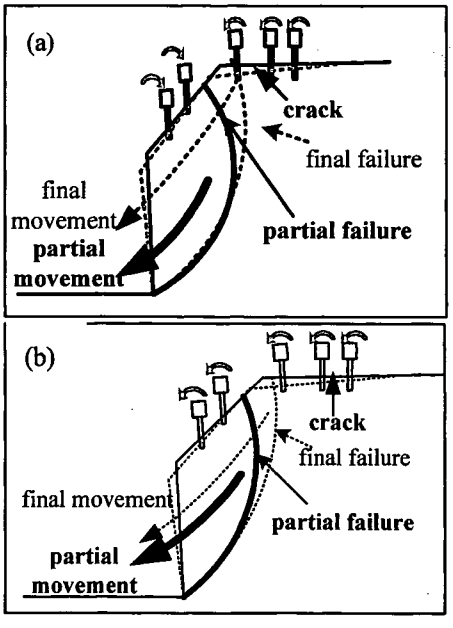

Fig. 7 Failure pattern in two types of soil models (a) Narita sand (H) and (b) Kanto loam (H).

Table 3 Ttilt angles measured along X-axis

Narita sand (H) (around 51 min. elapsed time)					
tilt-angle	1	2	3	4	5
SSC	-0.275	-0.11	0.25	-	0.025
SA	-0.300	-0.15	0.25	0.06	0.025
Kanto loam (H) (around 88 min. elapsed time)					
tilt angle	1	2	3	4	5
SSC	0.50	0.08	0.54	-	0.400
SA	0.50	0.30	0.50	1.08	0.150

of wet density of Narita sand (H) being higher than that of Kanto loam (H). This might be due to the difference in the effect of cohesion and angle of frictional resistance. Also, comparison between SSC and SA type tilt sensors for each soil are also made. Both SSC and SA tilt sensors showed almost same value. This shows the applicability of both types of tilt sensors in the field with equal efficiency. Little variation in SA and SSC tilt sensors for Kanto loam might have occurred due to the size of accelerometers, insertion depth, etc.

4. Conclusions

1) All types of tilt sensors gave good response during the excavation and just before the failure. They showed sharp increment just before the failure. Hence all types of sensors could be used to predict the failure movement during the excavation works.

2) Both SA and SSC tilt sensors used in each model slope showed almost same pattern and same amount of movement. This suggests that both SA and SSC tilt sensors could be used with equal efficiency in the field.

3) Determination of direction of resultant failure movement and failure pattern are possible with these new tilt sensors.

5. Acknowledgement

This work is partially carried out under the Health and Labor Sciences Research Grants of Ministry of Health, Labor and Welfare.

References

Tamrakar S.B., Toyosawa Y., Itoh K. and Ariki T.:「実大実験による法尻掘削に起因する斜面崩壊の前兆現象の検討」, 第３５回安全工学シンポジウム、pp. 319-322 (2005).

Relationship between critical failure height and trench excavation depth in relation to centrifuge tests performed with In-flight excavator

Ọ Tamrakar S.B., Toyosawa Y., Itoh K. and Timpong S. (Japan National Institute of Occupational Safety and Health)

1. Introduction

Most of the accidents take place during the excavation of lower parts of the slopes, especially the trenches (excavation below the toe level). Earlier Tamrakar et. al (2005) carried out the tests at centrifuge using in-flight excavator for volcanic sand with and without making trench excavations at the beginning and it was reported that the vertical height before the failure was larger for the excavation made without trench at the start of trench excavation than the excavation made with the trench. In this research, trench excavations are made at different distances from the toe of the slope along with the normal excavation and the effect of trench excavation on the failure height just before the failure was studied. Comparison of failure heights observed for the normal and combined excavations is made. With this, a better and safer position of trench excavation could be made. Also, stepwise sharp increment in displacement during the excavation and just before the failure with linear vertical differential transducer (LVDT) set up on the slope crest showed the possibility of prediction of failure in advance.

2. Preparation of Model Slope and Set Up

In this experiment, Narita sand collected from the Toke excavation site, Chiba prefecture, Japan was used. Physical properties, particle size distribution and direct shear test results of this soil is shown in Table 1. Soil specimen was thoroughly mixed with pre-determined water content (w) and kept in plastic bag for several days. Model slope ground from these soils was prepared in a model box (0.45 m x 0.20 m x 0.272 m), by statically compacting them into number of layers using bellofragm cylinder under 50 kPa. Thickness of each layer is about 0.02 m and compaction time for each layer was about 5 minutes. Model slope ground was then cut into required dimensions shown in Fig. 1 with fixed slope angle of 50 degree. This slope angle is lower than the one mentioned in the safety guideline of Labor Safety and Health Regulation. The lower and safer angle was selected so that longer slope length (i.e. distance of excavation from the toe of the slope) could be obtained which will facilitate to make trench excavations at different distances from the toe. Completed model slope along with model box was finally shifted to centrifuge platform. Direct contact type LVDT (D-1 to D-5) were placed on the top surface of the slope at 0.01, 0.04, 0.07, 0.105 and 0.142 m distances from the crest of the slope (Fig. 1). Once the set up of LVDT was finished, in-flight excavator (Toyosawa et. al, 1998) was positioned in the centrifuge platform in such a way that its blade could

Table 1. Properties of Narita sand

	Narita Sand
Unit weight of soil solid (kN/m^3)	26.12
0.075x10^{-3}~2x10^{-3}m (%)	77.5
0.005x10^{-3}~0.075x10^{-3}m (%)	12.7
<0.005x10^{-3}m (%)	9.8
Avg. particle size, D_{50} (x10^{-3}m)	0.1909
Soil classification	SF
Cohesion, c (kPa)	9.78
Angle of internal friction (ϕ°)	15.88

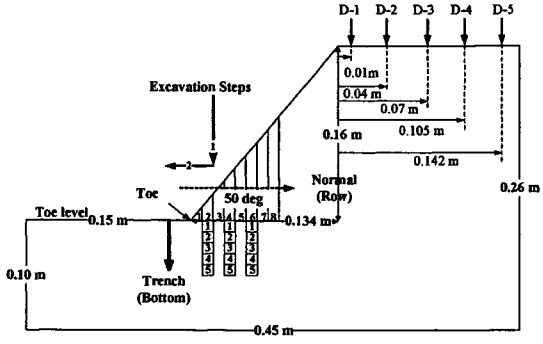

Fig. 1 Outline of model slope showing the positions of LVDTs on the slope top.

move freely within the model box.

3. Details of Centrifuge Model Tests

Experimental conditions for one normal and three combined excavations (normal + trench) are shown in Table 2. Each excavation (cut) was carried out vertically downward and outward from the slop.

In case of normal excavation, cutting was started from the slope surface to vertically downward and up to toe level. Width of each vertical cut of the model slope in normal excavation is 0.01 m. Each vertical cut (above the toe level) is represented by "Row (R)" and it is followed by the numbers as follows; R-1, R-2, R-3 and so on. R-1 represents the 1st cut, excavating at 0.01 m distance from the toe of the model slope. Similarly, R-2 and R-3 represent the second and third cuts, excavating the model slope at 0.02 and 0.03 m distances from the model slope toe, respectively. Combined excavation represents the trench excavation at particular normal cut (row). Trench excavation represents the vertical cut behind and below the toe level at particular Row (R). Depth of each cut of trench of model is fixed at 0.01 m and trench excavation is represented by "Bottom (B)" which is followed by numbers as follows; B-1, B-2, B-3, and so on. B-1 represents the cut at 0.01 m below from the toe level. Similarly, B-2 and B-3 represent the cuts at 0.02 and 0.03 m depths from the model slope toe level, respectively. During the normal excavation, model slope was failed at R-8-B-0. Hence combined excavations were carried within the range from the toe to this failure distance. Here, R-2, R-4 and R-6 were chosen to carry out the combined excavations. Each case of excavation is shown in Table 2. For example: R-2-B-5. This represents the width of normal cut behind and at the toe level is 0.02 m (i.e. at 0.02 m distance from the model slope toe) and depth of trench cut behind and below the toe level is 0.05 m; showing the excavation at 0.02 m distance from the toe and up to 0.05 m depth below the toe level.

Table 2. Experimental conditions for Narita Sand.

Type of excavation	Normal	Combined		
Cases	R8-B0	R2-B5	R4-B3	R6-B2
Bulk unit wt. (kN/m^3)	10.94	12.56	12.18	12.7
w (%)	9.89	10.75	9.22	9.22
Acceleration, G	31.3	31.3	31.6	31.8
Failure ht. (R) (m)	2.985	0.746	1.507	2.275
Failure depth (B) (m)	0	1.565	0.948	0.636
Critical failure ht. (m	2.985	2.311	2.455	2.911
H_{cr} (m)	3.576	3.115	3.211	3.079

In this research, height of the slope in the field from the toe level was assumed to be 5 m. But the slope height (height from the toe level to slope top) was 0.16 m (total height of the model is 0.26 m). Therefore to meet the slope height of 5 m, centrifuge acceleration was increased up to 31.3 G. Similarly, for other cases also acceleration was fixed in such a way that their real slope height becomes 5 m. Accelerations for each case are shown in Table 2. During the test, acceleration was increased gradually in steps from 5 ~ 10 ~ 15 ~ 20 ~ 25 ~ 31.3G. Once the vertical displacement become constant at 31.3G, then the excavation was started.

4. Test Results and Discussions

Excavation test results are shown in Table 2. In the table, all the values are changed into real field value by multiplying the data obtained from model test by the respective centrifuge acceleration values. 'Failure height' in table represents the height of slope above the toe level just before the failure. Similarly, 'Failure depth' represents the depth of trench cut below the toe level. 'Critical failure height' represents the summation of failure height and failure depth. Critical failure height is the maximum for normal cases and it reduces with the combined excavation near the toe. 'Critical height $[H_{cr}=(4*c)/\gamma_t]$)' shown in the Table 2 was calculated theoretically by using the equation where bulk unit weight and cohesion are used. Critical failure height obtained from the normal and combined excavation cases was smaller than those calculated theoretically. As theoretically obtained critical value is larger than those obtained from excavation, one should be careful while using the critical failure height as the reference during the excavation works.